Autofluorescent Organelles Within the Retinal Pigment Epithelium in Human Donor Eyes With and Without Age-Related Macular Degeneration

Katharina Bermond,[1] Leon von der Emde,[2] Ioana-Sandra Tarau,[3] Leonie Bourauel,[2] Rainer Heintzmann,[4,5] Frank G. Holz,[2] Christine A. Curcio,[6] Kenneth R. Sloan,[6] and Thomas Ach[2]

[1]Department of Ophthalmology, Ludwigshafen Hospital, Ludwigshafen, Germany
[2]Department of Ophthalmology, University Hospital Bonn, Bonn, Germany
[3]Department of Ophthalmology, University Hospital Würzburg, Würzburg, Germany
[4]Leibniz Institute of Photonic Technology, Jena, Germany
[5]Institute of Physical Chemistry and Abbe Center of Photonics, Friedrich-Schiller University Jena, Jena, Germany
[6]Department of Ophthalmology, University of Alabama at Birmingham, Alabama, AL, United States

Correspondence: Thomas Ach, FEBO, University Hospital Bonn, Ernst Abbe Straße 2, Bonn 53127, Germany;
thomas.ach@ukbonn.de.

KB and LE contributed equally and should be considered co-first authors.

Received: June 10, 2021
Accepted: December 22, 2021
Published: January 20, 2022

Citation: Bermond K, von der Emde L, Tarau IS, et al. Autofluorescent organelles within the retinal pigment epithelium in human donor eyes with and without age-related macular degeneration. *Invest Ophthalmol Vis Sci.* 2022;63(1):23. https://doi.org/10.1167/iovs.63.1.23

Purpose. Human retinal pigment epithelium (RPE) cells contain lipofuscin, melanolipofuscin, and melanosome organelles that impact clinical autofluorescence (AF) imaging. Here, we quantified the effect of age-related macular degeneration (AMD) on granule count and histologic AF of RPE cell bodies.

Methods. Seven AMD-affected human RPE-Bruch's membrane flatmounts (early and intermediate = 3, late dry = 1, and neovascular = 3) were imaged at fovea, perifovea, and near periphery using structured illumination and confocal AF microscopy (excitation 488 nm) and compared to RPE-flatmounts with unremarkable macula (n = 7, >80 years). Subsequently, granules were marked with computer assistance, and classified by their AF properties. The AF/cell was calculated from confocal images. The total number of granules and AF/cell was analyzed implementing a mixed effect analysis of covariance (ANCOVA).

Results. A total of 152 AMD-affected RPE cells were analyzed (fovea = 22, perifovea = 60, and near-periphery = 70). AMD-affected RPE cells showed increased variability in size and a significantly increased granule load independent of the retinal location (fovea: P = 0.02, perifovea: P = 0.04, and near periphery: P < 0.01). The lipofuscin fraction of total organelles decreased and the melanolipofuscin fraction increased in AMD, at all locations (especially the fovea). AF was significantly lower in AMD-affected cells (fovea: <0.01, perifovea: <0.01, and near periphery: 0.02).

Conclusions. In AMD RPE, lipofuscin was proportionately lowest in the fovea, a location also known to be affected by accumulation of soft drusen and preservation of cone-mediated visual acuity. Enlarged RPE cell bodies displayed increased net granule count but diminished total AF. Future studies should also assess the impact on AF imaging of RPE apical processes containing melanosomes.

Keywords: autofluorescence, lipofuscin, structured illumination microscopy, confocal fluorescence microscopy, melanosomes, melanolipofuscin

Retinal pigment epithelium (RPE) cells are essential for outer retinal health and play a key role in the pathogenesis of age-related macular degeneration (AMD). RPE cells absorb light, phagocytize photoreceptor outer segments, exchange metabolites with photoreceptors, and recycle retinoids of the visual cycle.[1] A hallmark of RPE cells is the presence of hundreds of granules relevant to clinical imaging via autofluorescence (AF; lipofuscin and melanolipofuscin) and optical coherence tomography (OCT; lipofuscin and melanolipofuscin, plus mitochondria); the vast majority of these organelles in any one cell are lipofuscin and melanolipofuscin.[2–4]

Lipofuscin and melanolipofuscin within the RPE are histologically detectable early in life.[5,6] The accumulation continues for decades resulting in increased RPE AF, both in histology and clinical imaging.[7,8] At advanced age and in AMD, AF granules demonstrate a characteristic histologic redistribution[9–11] that could also impact clinical AF imaging. Recently, alteration and loss of clinical AF signal have been identified as precursors of geographic atrophy,[12] consistent with this expectation. Quantitative autofluorescence (QAF), an in vivo imaging technique using a camera with an internal standard, revealed that AF levels in clinical fundus autofluorescence (FAF) of AMD eyes is

reduced. In a cohort of intermediate AMD eyes with large drusen,[13] QAF levels were reduced compared to healthy eyes and further decreased over time, confirming findings from other groups that AF intensity in AMD is generally decreased.[14,15]

Using high-resolution structured illumination microscopy (SIM), we previously imaged individual RPE granules exhibiting AF and further subdivided the major granule classes (lipofuscin, melanolipofuscin, and melanosomes) into nine different phenotypes.[4] In a recent survey of more than 195,000 RPE granules in young and aged human donor eyes with unremarkable maculae, lipofuscin was low at the fovea and increased with age and with eccentricity (highest at the perifovea).[4] Melanolipofuscin on the other hand was the major granule type in foveal RPE cell bodies and remained stable across the above-mentioned locations and over time.[4] However, it is valuable to the interpretation of clinical imaging to determine how the content of RPE cell granules and their intracellular distribution is impacted by AMD, as determined with the nine-phenotype classification system.

The purpose of this study was to three-dimensionally image human RPE cell bodies of AMD-affected donor eyes using high resolution SIM, characterize granule content, distribution, and correlate granules with AF. These histologic results will help to further clarify whether RPE cells and its granules are altered in the presence of AMD. In addition, our data will benefit the interpretation of clinical AF imaging in patients with AMD.

Methods

The protocols adhered to the Tenets of the Declaration of Helsinki and the study was approved by the Institutional Review Boards of the University of Alabama at Birmingham and the Ethics Committees of the University of Würzburg and the University of Bonn, Germany.

Tissue

For this study, seven previously documented AMD-affected human donor eyes were utilized.

Tissue preparation of human donor eyes has previously been described in detail.[7] Briefly, the globes were collected from the Advancing Sight Network (Birmingham, AL, USA) within 4.2 hours of death, prepared and preserved by immersion in 4% paraformaldehyde/0.1-M phosphate buffered saline, and inspected under a dissection microscope equipped with trans- and epi-illumination. The neuroretina and choriocapillaris were removed in a multistep preparation and imaging process to ensure preservation of the exact foveal position (for details, see Supplementary Fig. S1 in Ach et al.)[7] RPE-Bruch's membrane flat mounts were then imaged at three predefined locations using the regional definitions by Polyak[16]: fovea (0.4 ± 0.5 mm superior to the foveal center), perifovea (4.1 ± 0.2 mm superior to the foveal center), and near-periphery (8.6 ± 1.3 mm superior to the foveal center). These regions were chosen for the distinctive content of overlying photoreceptors (local rod:cone ratio 0, 17.5, approximately 25, respectively),[17,18] because RPE lipofuscin originates as ingested outer segments.

Imaging Protocol

For AMD RPE cell imaging, a commercially available SIM device (ELYRA-S.1; Carl Zeiss Microscopy, Jena, Germany) was used (excitation wavelength = 488 nm and emission = 510–750 nm). Images were captured using a 63X, numerical aperture 1.40, plan apochromat oil immersion objective and an iXon 885 EMCCD camera (Andor Technology Ltd., Belfast, Northern Ireland, UK), cooled to –63°C. Further SIM specifications (grid pattern and exposure times) have been published.[9] The scanning area of 75.56 × 75.40 μm^2 captured 20 to 25 RPE cells per location (for exceptions, see below). Z-stacks of SIM images were acquired from apical RPE (first granules in focus) to basal RPE (last granules out of focus) in 100-nm steps. SIM superimposes illumination grids on the tissues, and during imaging the grids are differently positioned and oriented. Each z-stack slab consisted of 15 raw images (5 grating positions × 3 rotations of the illumination grid). All slabs were postprocessed to extract and reconstruct the high-resolution images (device's internal software, ZEN 2010).

At each location (fovea, perifovea, and near-periphery), adjacent RPE cells were selected from reconstructed SIM images based on visibility of cell boundaries (tiny gaps between two adjacent cells at the basolateral side, visible while scrolling through the z-stack). RPE cell borders were identified by a granule free void between RPE cells, as the RPE cell border and tight junctions do not display AF properties (see Supplementary Fig. S1). At locations severely affected by AMD, adjacent cells were not detectable in all cases due to loss of cell boundaries and the presence of giant and, in some cases, multinucleate RPE cells. Therefore, for the fovea, instead of using individual RPE cells, areas equal to the size of 10 foveal RPE cells were analyzed (169 μm^2, equivalent to the area of an average foveal healthy cell) in some cases. Due to loss of cell boundaries at the perifovea in one tissue (late exudative AMD), we also analyzed a predefined area instead of individual cells (217 μm^2, equivalent to the area of an average perifoveal healthy cell; 14% of perifoveal AMD cells were analyzed in this manner).

Image Analysis and Granule Classification

For image analysis and granule subclassification, we used custom written FIJI plugins.[19] A demarcation line was manually drawn with computer assistance around each cell within the reconstructed SIM images, and cell area and height (number of z-stack slabs × 100-nm step size) were reported. RPE cell borders were identified by a granule free void between RPE cells, as the RPE cell border and tight junctions do not display AF properties. A custom FIJI plugin was used for recording granule counts and classifications made by human observers (code for the plugin, TA_Pick_Particles, is available online, http://sites.imagej.net/CreativeComputation). To further highlight possible differences in apical and basal granule distribution, RPE cells were partitioned into four equally sized apical-to-basal quartiles (Q1–Q4), where Q1 to Q3 covered the cushion of granules visible on SIM images and Q4 was known to contain abundant non-AF mitochondria.[3,4]

All identifiable granules within the selected RPE cell bodies were manually tagged with computer assistance and independently classified by one of two trained graders on the basis of granule morphology (see below). While the

Investigative Ophthalmology & Visual Science

observer scrolled through the z-stacks, the center of each granule was marked with a dot in the slab that revealed the maximum granule dimension. Typically, granules expanded over 6 to 8 slabs corresponding to an average granule size of about 1 µm. Previously marked granules were automatically displayed in preceding and subsequent slabs to avoid duplicate assignments. For each tagged granule, the classification code (see below) and its x, y, z coordinates within the stack were registered and written to a text file for further statistical analysis. However, granule marking was done manually; the plugin served only to record the coordinates.

Granule Types

Granule type characterization was carried out as previously described in healthy RPE cells.[4] There, we defined a total of 9 different granule phenotypes: lipofuscin 1, uniform lipofuscin granules and lipofuscin 2, conglomerates (variable-shaped accumulation of hyper-AF material with irregular intragranular AF patterns, larger than lipofuscin 1); melanolipofuscin 1, melanolipofuscin with complete AF coating and minimal AF in the center; melanolipofuscin 2, melanolipofuscin with complete AF coating and hypo- to iso-AF in the center; melanolipofuscin 3, melanolipofuscin with incomplete AF coating; melanolipofuscin 4, bull's-eye-shaped melanolipofuscin with complete AF coating and AF core; and melanolipofuscin 5, large round melanolipofuscin granules with AF coating (greater than twice the volume of a typical lipofuscin granule). Due to a limited inter-reader agreement in the distinction among melanolipofuscins 1 to 3 in our previous work, results for these three subtypes were pooled (see below). Finally, in line with recent distinction of melanosomes from organelle mapping studies, round (melanosome 1) and spindle-shaped (melanosome 2) melanosomes could be detected, neither of which showed notable AF components on the surface nor the granule body.[2–4] For analysis, results for melanolipofuscins 1 to 3, melanosomes 1 to 2, and lipofuscins 1 and 2 were each pooled.

Determination of Total Autofluorescence Per Cell

In addition to SIM imaging, using a Zeiss LSM 780 laser scanning confocal fluorescence microscope (excitation = 488 nm, emission = 490–695 nm, and 24 channels, 8.9-nm spectral channel width), flat mounts were imaged at the identical locations documented in SIM imaging. Cells were imaged from the apical aspect (first granules in focus) to the basal aspect (last granules out of focus) in 390-nm steps and total AF/cell was determined as previously described.[4] The scanning area covered 224.92 × 224.92 µm^2. Laser scanning microscopy (LSM) was performed before SIM imaging, because of the possible bleaching effects due to longer and more intense laser power in SIM.[4] The AF settings were identical between donors and retinal location, however, analyses of total AF have to be interpreted cautiously as no reference AF bar has been used.

Statistical Analysis

Statistical analyses were achieved in the software environments R (R Foundation for Statistical Computing, IBM) and SPSS. A mixed effect analysis of covariance (ANCOVA; between effect: presence of AMD; within effect: cells nested in participant; and covariate: age) was implemented to analyze the effect of AMD on the total number of granules (log transformation to reach log-normal distribution), granule density and AF in the fovea, perifovea, and near periphery respectively. ANCOVA was followed up by Mauchly's sphericity test and, if necessary, a Greenhouse-Geisser test for validation. We correlated granule count with cell area, and AF with granule count and cell area using the Spearman correlation coefficient.

Results

Seven RPE flat mounts from seven donor eyes (4 women and 3 men, mean age ± SD = 85 ± 3 years, and range = 81–90 years) with three early/intermediate, one late dry, and three neovascular AMD manifestation were included. A total

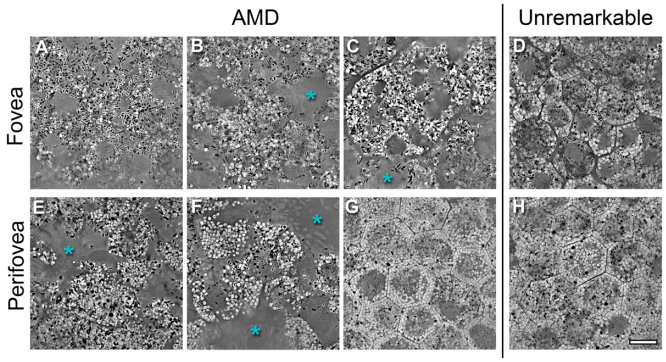

Figure 1. SIM-images of AMD-affected and unremarkable tissue. Each image shows a representative slide at the apical surface of a SIM z-stack of the fovea (**A–D**) or perifovea (**E–H**) of AMD-affected (**A–C, E–G**) or unremarkable (**D, H**) tissues. The AMD-affected tissues show deterioration of cell structures like dissolving cell borders, partial loss of intracellular granule organization and cell loss. Areas of RPE cell loss probably associated with deposits (basal laminar deposits/basal linear deposits) are marked with a *blue asterisk*. These deposits affected the fovea and, in some tissues, extended to the perifovea (**E, F**). Where the perifovea was not (yet) affected by AMD (**G**), the tissue appeared comparable to healthy tissue (**D, H**) which shows uniform cell shapes and orderly intracellular granule distribution. Note: the granule free areas within the cell bodies in **D** and **H** represent the non-autofluorescent cell nucleus. In panels **A**, **B**, and **E**, we were unable to distinguish cell boundaries and used cell-size equivalent squares instead. A 3D-version of panel **C** is further depicted in the supplemental video. Early or intermediate AMD: 83-year-old woman (**F**), 84-year-old man **B**, and 86-year-old woman **A**. Late non-exudative AMD: 81-year-old man **C, G**. Late exudative AMD: 90-year-old woman **E**. Unremarkable tissue: 83-year-old woman **D** and 90-year-old woman **H**. Scale bar = 10 µm.

Investigative Ophthalmology & Visual Science

of 152 RPE cells (or equivalent squares) at the 3 canonical locations were analyzed (fovea = 22 cells, perifovea = 60 cells, and near-periphery = 70 cells; Fig. 1).

Fovea

Data from foveal RPE are available from four donors. One eye with early/intermediate AMD showed a giant RPE cell with densely packed granules and no apparent nuclei; one eye with late non-exudative AMD also showed a giant RPE cell at the fovea with 12 nuclei and/or vacuoles. In 2 donor eyes, no RPE cell boundaries could be distinguished, and analysis was based on 10 cell size equivalent squares each (see below, 90% of foveal AMD cells were analyzed in this manner). The three donor eyes with late exudative AMD with macular atrophy in addition to neovascularization showed no remaining RPE tissue at the fovea and, therefore, were excluded from analysis.

The SIM scanned foveal areas (Fig. 2) from the 2 donors were analyzed within 20 squares, each equivalent to the area of a typical RPE cell in a healthy fovea. These squares displayed a total granule load per square of 613 ± 267, which was significantly increased compared to healthy aged foveal RPE cell of the same size (339 ± 137; P value/η^2 value: 0.02/0.31; Tables 1, 2). Melanolipofuscin granules were the dominant population (lipofuscin = 111 ± 58 and melanolipofuscin = 497 ± 278 (no melanolipofuscin 4 and no melanolipofuscin 5; and melanosome, 5 ± 6 (see Table 1). Percentage-wise fractional distribution showed a reduced lipofuscin fraction compared to healthy aged cells (Table 3). Intracellular spatial granule distribution showed a slightly increased granule load in the central quartile (Q2) compared to healthy cells (AMD/healthy Q2: 49%/44% fractional granule load).

Of note, two foveae of two donors revealed significantly enlarged cells (see one in the Supplementary Video). In a donor with early/intermediate AMD, one cell demonstrated a total granule load of 4624 granules (751 lipofuscin, 3820 melanolipofuscin, and 53 melanosomes), whereas no nucleus could be identified. In a donor with late non-exudative AMD, one cell displayed a total granule load of 3785 granules (1384 lipofuscin, 2386 melanolipofuscin, and 15 melanosomes). Twelve spherical non-autofluorescent areas were identified in this cell. These could be nuclei, vacuoles, or both.

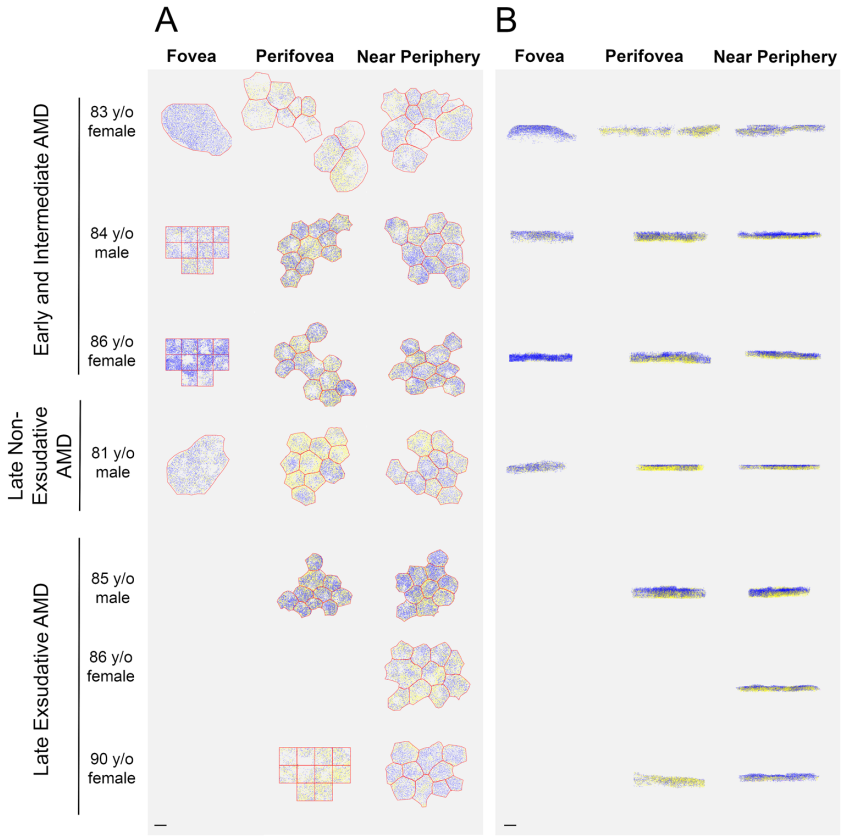

Figure 2. En face (A) and cross section (B) view of intracellular granule distribution. Each analyzed granule was color-coded and plotted (lipofuscin: *yellow*, melanolipofuscin 1–3: *blue*, melanolipofuscin 4: *pink*, melanolipofuscin 5: *magenta*, and M: *orange*). Only few melanosomes, melanolipofuscin 4, and melanolipofuscin 5 were detectable. *Red lines* represent cell borders or artificial squares, respectively. At four locations (three foveae and one perifovea), no granule analysis was possible due to large RPE-atrophy. Foveal tissue showed distinctive alterations in cell structure with either formation of enlarged cells (83-year-old woman and 81-year-old man) or primarily faded cell borders and a moth-eaten appearance (84-year-old man and 86-year-old woman [early/intermediate AMD]). The predominant granule type at the fovea remained melanolipofuscin, like in unremarkable tissues.[4] At the perifovea and near periphery, all tissues that showed a regular cell structure in the en face view also displayed two bands in the cross-section view: an apical band with predominantly melanolipofuscin and lipofuscin and a basal band with predominantly lipofuscin. At locations where the cell structures were deteriorated (83-year-old perifovea and near periphery, 90-year-old perifovea) these two bands could not be distinguished. Scale bar = 10 µm.

Investigative Ophthalmology & Visual Science

Table 1. Number of Granules and Mean Cell Area in AMD and Normal Aged RPE Cells[4]

		Location		
	Type	**Fovea (n = 20)**	**Perifovea (n = 60)**	**Near Periphery (n = 70)**
All granules	AMD	613 ± 267	1069 ± 507	956 ± 380
	Normal aged	339 ± 137	508 ± 194	522 ± 316
Lipofuscin, all types	AMD	111 ± 58	580 ± 270	418 ± 208
	Normal aged	106 ± 78	318 ± 152	293 ± 261
Melanolipofuscin, all types	AMD	497 ± 278	486 ± 302	535 ± 229
	Normal aged	228 ± 84	189 ± 76	226 ± 89
Melanolipofuscin 4	AMD	0	1 ± 2	2 ± 3
	Normal aged	0	1 ± 1	3 ± 3
Melanolipofuscin 5	AMD	0	3 ± 3	3 ± 3
	Normal aged	1 ± 1	2 ± 2	3 ± 3
Melanosomes	AMD	5 ± 6	3 ± 3	3 ± 4
	Normal aged	4 ± 5	2 ± 3	2 ± 3
Cell area, μm^2	AMD	1758 ± 23	235 ± 116	249 ± 98
	Normal aged	174 ± 5	216 ± 66	215 ± 90

Please note, the cell area in the fovea is only listed for the two enlarged cells as in other cases size-equivalent squares were used. Reported are means ± standard deviation.

Table 2. Granule Composition in Different AMD Disease Manifestations. Reported are Number of Granules Per Cell ± Standard Deviation

		Location	
Granule Type	**AMD Stage**	**Perifovea**	**Near Periphery**
All	Early/intermediate	1136 ± 513	969 ± 383
	Late exudative	1017 ± 598	976 ± 421
	Late non-exudative	973 ± 225	819 ± 213
Lipofuscin	Early/intermediate	602 ± 299	400 ± 173
	Late exudative	508 ± 265	437 ± 244
	Late non-exudative	658 ± 145	419 ± 216
Melanolipofuscin, all types	Early/intermediate	531 ± 267	566 ± 238
	Late exudative	507 ± 367	536 ± 230
	Late non-exudative	311 ± 200	394 ± 103
Melanolipofuscin 4	Early/intermediate	1 ± 2	2 ± 2
	Late exudative	2 ± 2	2 ± 4
	Late non-exudative	1 ± 1	1 ± 1
Melanolipofuscin 5	Early/intermediate	2 ± 2	3 ± 3
	Late exudative	2 ± 2	3 ± 4
	Late non-exudative	6 ± 5	4 ± 3
Melanosomes	Early/intermediate	3 ± 3	3 ± 3
	Late exudative	2 ± 2	2 ± 3
	Late non-exudative	5 ± 3	6 ± 6

Table 3. Granule Distribution at the Fovea, Perifovea, and Near Periphery

		Location		
	Type	**Fovea**	**Perifovea**	**Near Periphery**
Lipofuscin, all types	AMD	21.1%	54.3%	43.8%
	Normal aged	31.4%	62.5%	56.2%
Melanolipofuscin, all types	AMD	78.1%	45.1%	55.4%
	Normal aged	67.2%	36.5%	42.3%
Melanolipofuscin 4	AMD	0.1%	0.1%	0.2%
	Normal aged	<0.1%	0.3%	0.6%
Melanolipofuscin 5	AMD	<0.1%	0.3%	0.4%
	Normal aged	0.1%	0.4%	0.5%
Melanosomes	AMD	0.8%	0.3%	0.3%
	Normal aged	1.3%	0.4%	0.4%

Investigative Ophthalmology & Visual Science

Table 4. Granule Density at the Fovea and Perifovea

Granule Type	AMD Stage	Location: Granules/100 mm²		
		Fovea	Perifovea	Near Periphery
All	Early/intermediate	345 ± 161	503 ± 254	402 ± 184
	Late exudative	NA	593 ± 369	438 ± 239
	Late non-exudative	217	419 ± 44	348 ± 29
Lipofuscin	Early/intermediate	64 ± 33	259 ± 127	166 ± 86
	Late exudative	NA	285 ± 141	191 ± 116
	Late non-exudative	79	287 ± 51	174 ± 55
Melanolipofuscin	Early/intermediate	278 ± 167	243 ± 145	234 ± 109
	Late exudative	NA	306 ± 237	246 ± 142
	Late non-exudative	137	130 ± 65	171 ± 44
Melanosomes	Early/intermediate	2 ± 3	1 ± 2	1 ± 1
	Late exudative	NA	1 ± 1	1 ± 1
	Late non-exudative	1	1 ± 1	2 ± 2

NA, not applicable.

Due to the limitations of using cell-size equivalent squares at the fovea we further reported 2D granule density (granule/area = 100 µm²; Table 4). Granule density was not significantly increased compared to healthy aged cells (*P* value/η^2 value: 0.07/0.8).

Perifovea

The perifovea revealed the highest total granule load per cell among all three locations. Cells had 1069 ± 507 granules within their cell body, significantly more than in healthy aged perifoveal cells (508 ± 194, *P* value/η^2 value of 0.04/0.37). Granule density (see Table 4) was not significantly increased compared to healthy aged cells (*P* value/η^2 value: 0.6/0.16). Cells contained 580 ± 270 lipofuscin, 486 ± 302 melanolipofuscin (1 ± 2 melanosomes 4 and 3 ± 3 melanolipofuscin 5), and 3 ± 3 melanosomes on average (see Table 1).

Granule load varied among AMD manifestations with 1136 ± 513 (early/intermediate), 1017 ± 598 (late exudative), and 973 ± 225 (late non-exudative AMD; see Table 2). Percentage-wise granule distribution showed an increase in the melanolipofuscin fraction compared to the unaffected macula (see Table 3). Intracellular spatial granule distribution was in line with aged healthy cells with melanolipofuscin, melanolipofuscin 4, and melanosomes found mainly in Q1 (apically) and lipofuscin and melanolipofuscin 5 distributed mainly in the Q2 and Q3 (basolateral).

Near Periphery

The total granule load per cell at the near periphery was 956 ± 380, which was significantly higher than healthy aged cells at the near periphery (522 ± 316; *P* value/η^2 value <0.01/>0.37). Granule load varied among AMD manifestations (early/intermediate, late exudative, and late non-exudative AMD) with (mean ± SD) 969 ± 383, 976 ± 42, and 819 ± 213, respectively (see Table 2). Cells were composed of 418 ± 208 lipofuscin, 535 ± 229 melanolipofuscin (melanolipofuscin 4, 2 ± 3; melanolipofuscin 5, 3 ± 4), and 3 ± 4 melanosomes granules (see Table 1). Intracellular spatial granule distribution mimicked healthy aged RPE cells with melanolipofuscin, melanolipofuscin 4, and melanosomes found rather apically (Q1) and lipofuscin and melanolipofuscin 5 mainly spread in the basolateral quartiles (Q2 and Q3).

RPE Morphology

Cell areas (Fig. 3) were markedly increased in AMD RPE cells with an average area of 265 ± 213 µm² compared to 201 ± 73 µm² for healthy aged cells. Cells of the near periphery (249 ± 98 µm² in AMD versus 215 ± 90 µm² in healthy aged eyes) were slightly larger than perifoveal cells (235 ± 116 µm² in AMD versus 216 ± 66 µm² in healthy aged eyes). Two giant RPE cells (1.3% of all RPE cells) found in each of two foveae were 1775 µm² and 1742 µm², respectively, and were about 10 times larger than the average normal aged foveal RPE cell (174 ± 5 µm²). Although these cells were grossly enlarged and densely packed with granules, these were the only two giant cells encountered. Total granule load was significantly associated with cell area, with a Spearman correlation coefficient 0.62 ($P = 0.02$).

RPE Autofluorescence Per Cell

RPE cells (and cell equivalent squares) in AMD had a significantly lower total AF as compared to healthy eyes at all three locations, after correcting for age (*P* value/η^2 value; fovea: <0.01/0.85; perifovea: <0.01/0.68; and near periphery: 0.02/0.25). These differences occur despite AMD cells being larger and having a higher overall granule load (see above). The two large cells at the fovea (not included in the analysis above) demonstrated increased AF/µm² compared to cell area equivalent AMD squares.

Discussion

This study compares RPE AF granule counts and AF intensity at predefined retinal locations from donor eyes with AMD to values in unaffected donor eyes. We found significantly decreased AF despite increased granule load in human RPE cells, as compared to RPE cells from healthy macula. Furthermore, granule load correlated with cell area. AMD cells demonstrated a tendency to be enlarged. We demonstrated an increase in total granule load in AMD independent of retinal location and AMD manifestation. At the same time, an increased variance of granule load in AMD RPE cells was reported, especially at the fovea, an area essential for cone

Investigative Ophthalmology & Visual Science

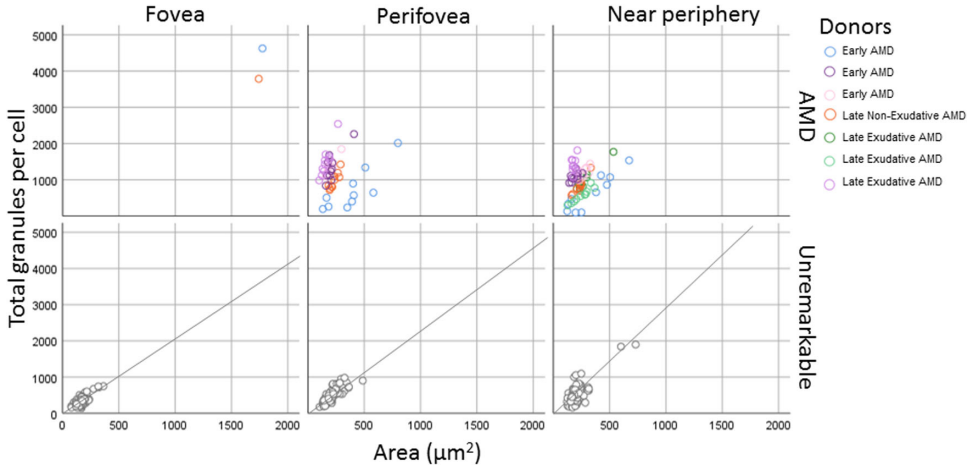

Figure 3. Granule load per cell area. The graph shows the area (x-axis) and total granule load (y-axis) of RPE cells from donors with age-related macular degeneration (*top row*) and aged donors with unremarkable macula (*bottom row*). Whereas aged RPE cells displayed a clear trend between cell area and granule load, AMD RPE cells demonstrated a dissociation between the two. Using repeated measures correlation to adjust for the dependence of different cells from one tissue we found a strong correlation between cell area and granule load in AMD RPE cells as well (perifovea: r = 0.77 [95% confidence interval [0.61, 0.87], *P* value < 0.001/near periphery: r = 0.86 [95% confidence interval 0.78, 0.91] *P* value < 0.001). These results show that the relationship for granule load and cell area is stronger within-tissue than between-tissue. RPE cells in AMD presented an increased cell area and granule load. This trend was most pronounced at the fovea. The graph also illustrates an increased variability in cell area and granule load in AMD.

mediated vision[20,21] yet also prone to the accumulation of soft drusen.[22,23]

Our published high-resolution imaging studies of RPE cells[4] demonstrated an increase of lipofuscin and melanolipofuscin with age in adulthood, confirming Feeney's early data showing increase of granules during aging, despite methodological differences. It is important to mention that studies using QAF have found that AF might decrease in participants over the age of 60 years.[12] However, our previous studies using histology as well as studies displaying marked differences of QAF dependent on lens opacification challenge this theory.[7,24] A decrease in QAF at higher age (>80 years), however, is possible but remains to be tested. In AMD, however, the relationship is not as straightforward. RPE cells in AMD show granule aggregation and subsequent basolateral shedding of granule aggregates, a phenomenon uniquely attributed to AMD so far.[9]

The major granule types (lipofuscin, melanolipofuscin, and melanosomes) revealed a tendency for proportionally reduced lipofuscin and increased melanolipofuscin in AMD. Granule subtypes were proportionally nearly equal, with lipofuscin 1 and melanolipofuscins 1 to 3 being the common determined granules. Our finding of proportionally decreased lipofuscin in AMD supports recent reports of lipofuscin redistribution and a probable loss in AMD rather than excessive accumulation.[9] The histological loss of lipofuscin with subsequent reduced or loss of AF in AMD RPE cells was independent of retinal location and persisted after correcting for age, and comports with clinical imaging. Several groups have shown reduced AF levels in patients with AMD using quantitative FAF, a phenomenon not attributable to light-blocking subretinal drusenoid deposits because AF is also reduced in eyes with sub-RPE drusen.[12,15,25] Therefore, it is most likely that the decrease in AF is due to changes at the RPE level. Photoreceptors are also impacted by AMD. Photoreceptor damage can result in increased AF signal, if light absorbing photopigment from photoreceptor outer segments is reduced or missing, as shown in AMD and other retinal diseases.[26–28]

We propose three different explanations for the increased granule load and the proportional change of lipofuscin and melanolipofuscin in AMD cells. First, AMD cells were shown to increase in size and to lose their typical shape, further underscored by our previous findings of vastly increased RPE cell areas in AMD without RPE cell loss.[9] Thus, we could have misjudged granule density if the cells' most apical and basal parts were out of focus and the cytoskeleton had not been labelled to define the actual cell dimensions. Future studies using alternative imaging techniques should focus on determining lipofuscin density in a 3D RPE cell depiction.

Second, the AF signal could be derived mainly from certain molecular components or granule subtypes rather than all of lipofuscin and melanolipofuscin.[29] Mass spectrometry studies revealed differing lipid signals in RPE cells dependent on retinal locations.[30] Topography of AF and photoreceptors are congruent with increased AF in areas of high rod density.[17,31] Further, it has been shown that rod mediated vision loss precedes and exceeds those of cones.[32–34] Therefore, it is possible that RPE cells demonstrate an overall increased granule load but with essential fluorophores for AF (possibly derived from rod outer segments) missing, changed, or not detectable in the short wavelength AF. Identifying the fluorophore(s) driving the FAF signal is pivotal for interpretation of AF in AMD.

Third, melanosomes, preferentially localized in the apical processes of RPE cells,[2,35] may shadow AF of more posteriorly localized lipofuscin and melanolipofuscin. At this point, however, no data are available on how AMD affects apical processes and melanosome load. It is believed that melanosomes are at least partly responsible for the near infrared (NIR)-AF signal.[36–38] So, future NIR-AF imaging and electron microscopy studies may help to elucidate differential melanosome compositions in the apical processes and

cell bodies of AMD affected RPE cells, as 488 nm excitation does not display melanosome AF properties.

The finding of a changed lipofuscin/melanolipofuscin ratio in AMD eyes also impacts the ongoing debate of lipofuscin's role in AMD progression. If the natural course of RPE cells in AMD is to re-organize the intracellular granule distribution with subsequent lipofuscin granule loss, to shift granule ratio toward melanolipofuscin, or both, then all these mechanisms give the impression of RPE cells trying to reduce lipofuscin load. An alternative hypothesis, however, would be that lipofuscin reduction and loss is not the cause but the consequence of other known (presence of basal laminar deposit and soft drusen material)[39–42] and unknown mechanisms that impact RPE cell integrity and function. Whether any intervention from outside is beneficial to therapeutically remove or reduce lipofuscin in AMD is under debate (Fang et al. ARVO abstract 2017, Investigative Ophthalmology & Visual Science, 58(8), 256–256).[43–46] In addition, as shown earlier, the increase of lipofuscin in normal aging does not impact the RPE cell morphology and supports lipofuscin's role as a pigment of aging and indicator of RPE cell health.[7]

Melanolipofuscin's role in RPE cells remains unclear. By SIM, melanolipofuscin was shown to be the most abundant granule type in normal and AMD foveal RPE cells, whereas in RPE cells at the perifovea and near periphery lipofuscin is prominent.[4] In addition, a sequence of granule conversion from melanosomes to melanolipofuscin to lipofuscin has been proposed by Feeney,[6] and recently revised.[4] Whether melanolipofuscin are an intermediary step in this sequence or an independent granule type needs further investigation. Spectral analysis of individual granules is currently in progress and will further contribute to the knowledge on individual granule types' role in RPE physiology. Changes in RPE cell morphometry and cell area at the areas heavily affected by AMD are probably related to cell fusion and/or failed cytokinesis.[47,48] This hypothesis is underscored by a body of evidence showing multinucleate RPE cells in AMD at the fovea, an area void of multinucleate RPE cells in healthy eyes.[48–50]

The granule increase in AMD affected RPE cells could be a response to local pathology, which also impacts RPE cell morphology (displacement and compression of RPE cells) especially in areas of drusen[39,51] or macular neovascularization.[52] Future studies combining in vivo clinical imaging like OCT with histology may help better explain the great variance in RPE cells at distinct AMD lesions.

Strengths of this study include imaging with well-preserved RPE flat mounts with short post-mortem time,[7] a large cohort of healthy RPE donor cells for comparison, and high-resolution SIM visualizing AF of individual RPE granules.[9] Limitations of our study include AF excitation of only one wavelength (488 nm)[36] with lack of information on other excitable fluorophores at different wavelengths, RPE cells restricted to 10 cells per location with analysis limited to three retinal locations, and imaging confined to the RPE cell body only due to possible loss of RPE's apical processes and indwelling organelles during processing. Nonetheless, the low numbers of melanosomes found within the cell body of this study is striking and further underscores the role of RPE's apical processes in housing melanosomes and contributing to clinical NIR-AF imaging. Further, analysis of cell area, 3D granule load and shape were hindered by missing RPE cells and the use of squares with average RPE cell size in some locations and donors. This could have possibly skewed reported total number of granules. We therefore consider data in Table 3 as the most indicative of changes from healthy to AMD pathology. In addition, no information on RPE cells responsible for intraretinal hyper-reflective foci (anteriorly migrating RPE cells) is available, which are an important OCT risk factors for AMD progression in multiple studies.[53–56] Finally, difficulties in delimiting RPE cells at the fovea do not allow proper comparison between disease manifestation, but also substantiate that RPE cells are altered most at this region. Comparison between disease manifestations is further hindered by the fact that eyes with exudative AMD also displayed macular atrophy impeding analyses of possible different disease pathways of these two late-stage AMD manifestations. Future histologic imaging studies should also include a reference for quantification of AF intensities across tissues and retinal locations. This would facilitate further clinical-histologic comparison to clinical QAF imaging.

In summary, compared to healthy RPE cells, RPE cells in AMD display reduced AF (excitation with 488 nm), increased total granule load, and an increased variance in granule load. These seemingly paradoxical findings can be explained by a combination of cell enlargement, possible cell fusion, and different proportions of granule subtypes and/or fluorophores.[51] This study helps to corroborate clinical (Q)AF studies in AMD and guide future interventional approaches in AMD affecting granule composition and new imaging biomarkers.

Acknowledgments

Supported by Dr. Werner Jackstädt Foundation (TA) and NIH/NEI 1R01EY027948-01 (T.A. and C.A.C.); human eye tissues were supported by NIH/NEI R01EY06109 (C.A.C.).

Disclosure: **K. Bermond**, None; **L. von der Emde**, None; **I.-S. Tarau**, None; **L. Bourauel**, None; **R. Heintzmann**, None; **F.G. Holz**, Acucela (C, F), Allergan (F), Apellis (C, F), Bayer (C, F), Boehringer-Ingelheim (C), Bioeq/Formycon (F, C), CenterVue (F), Ellex (F), Roche/Genentech (C, F), Geuder (C, F), Graybug (C), Gyroscope (C), Heidelberg Engineering (C, F), IvericBio (C, F), Kanghong (C, F), LinBioscience (C), NightStarX (F), Novartis (C, F), Optos (F), Oxurion (C), Pixium Vision (C, F), Oxurion (C), Stealth BioTherapeutics (C), Zeiss (F, C); **C.A. Curcio**, Genentech (F), Regeneron (F), MacRegen Inc. (I); **K.R. Sloan**, MacRegen Inc. (I); **T. Ach**, Roche (C), Novartis (C), Novartis (R), MacRegen Inc. (I)

References

1. Strauss O. The retinal pigment epithelium in visual function. *Physiol Rev*. 2005;85(3):845–881.
2. Pollreisz A, Messinger JD, Sloan KR, et al. Visualizing melanosomes, lipofuscin, and melanolipofuscin in human retinal pigment epithelium using serial block face scanning electron microscopy. *Exp Eye Res*. 2018;166:131–139.
3. Pollreisz A, Neschi M, Sloan KR, et al. Atlas of Human Retinal Pigment Epithelium Organelles Significant for Clinical Imaging. *Invest Ophthalmol Vis Sci*. 2020;61(8):13.
4. Bermond K, Wobbe C, Tarau I-S, et al. Autofluorescent Granules of the Human Retinal Pigment Epithelium: Phenotypes, Intracellular Distribution, and Age-Related Topography. *Invest Ophthalmol Vis Sci*. 2020;61(5):35.
5. Feeney-Burns L, Hilderbrand ES, Eldridge S. Aging human RPE: morphometric analysis of macular, equatorial, and peripheral cells. *Invest Ophthalmol Vis Sci*. 1984;25(2):195–200.

6. Feeney L. Lipofuscin and melanin of human retinal pigment epithelium. Fluorescence, enzyme cytochemical, and ultrastructural studies. *Invest Ophthalmol Vis Sci*. 1978;17(7):583–600.
7. Ach T, Huisingh C, McGwin GJ, et al. Quantitative autofluorescence and cell density maps of the human retinal pigment epithelium. *Invest Ophthalmol Vis Sci*. 2014;55(8):4832–4841.
8. Greenberg JP, Duncker T, Woods RL, Smith RT, Sparrow JR, Delori FC. Quantitative fundus autofluorescence in healthy eyes. *Invest Ophthalmol Vis Sci*. 2013;54(8):5684–5693.
9. Ach T, Tolstik E, Messinger JD, Zarubina A V, Heintzmann R, Curcio CA. Lipofuscin redistribution and loss accompanied by cytoskeletal stress in retinal pigment epithelium of eyes with age-related macular degeneration. *Invest Ophthalmol Vis Sci*. 2015;56(5):3242–3252.
10. Gambril JA, Sloan KR, Swain TA, et al. Quantifying retinal pigment epithelium dysmorphia and loss of histologic autofluorescence in age-related macular degeneration. *Invest Ophthalmol Vis Sci*. 2019;60(7):2481–2493.
11. Holmen IC, Aul B, Pak JW, et al. Precursors and development of geographic atrophy with autofluorescence imaging: Age-Related Eye Disease Study 2 Report Number 18. *Ophthalmol Retin*. 2019;3(9):724–733.
12. Reiter GS, Hacker V, Told R, et al. Longitudinal changes in quantitative autofluorescence during progression from intermediate to late age-related macular degeneration. *Retina*. 2021;41(6):1236–1241.
13. Emde L von der, Guymer RH, Pfau M, et al. Natural History of Quantitative Autofluorescence in Intermediate Age-Related Macular Degeneration. *Retina*. 2021;41(4):694–700.
14. Gliem M, Muller PL, Finger RP, McGuinness MB, Holz FG, Charbel Issa P. Quantitative Fundus Autofluorescence in Early and Intermediate Age-Related Macular Degeneration. *JAMA Ophthalmol*. 2016;134(7):817–824.
15. Orellana-Rios J, Yokoyama S, Agee JM, et al. Quantitative Fundus Autofluorescence in Non-Neovascular Age-Related Macular Degeneration. *Ophthalmic Surg Lasers Imaging Retina*. 2018;49(10):S34–S42.
16. Polyak S. *The Retina: The Anatomy and the Histology of the Retina in Man, Ape, and Monkey, Including the Consideration of Visual Functions, the History of Physiological Optics, and the Histological Laboratory Technique*. Chicago, IL: The University of Chicago Press; 1941.
17. Curcio CA, Sloan KR, Kalina RE, Hendrickson AE. Human photoreceptor topography. *J Comp Neurol*. 1990;292(4):497–523.
18. Curcio CA, Millican CL, Allen KA, Kalina RE. Aging of the human photoreceptor mosaic: evidence for selective vulnerability of rods in central retina. *Invest Ophthalmol Vis Sci*. 1993;34(12):3278–3296.
19. Schindelin J, Arganda-Carreras I, Frise E, et al. Fiji: an open-source platform for biological-image analysis. *Nat Methods*. 2012;9(7):676–682.
20. Pollreisz A, Reiter GS, Bogunovic H, et al. Topographic Distribution and Progression of Soft Drusen Volume in Age-Related Macular Degeneration Implicate Neurobiology of Fovea. *Invest Ophthalmol Vis Sci*. 2021;62(2):26.
21. Curcio CA. Soft Drusen in Age-Related Macular Degeneration: Biology and Targeting Via the Oil Spill Strategies. *Invest Ophthalmol Vis Sci*. 2018;59(4):AMD160–AMD181.
22. Thoreson WB, Dacey DM. Diverse Cell Types, Circuits, and Mechanisms for Color Vision in the Vertebrate Retina. *Physiol Rev*. 2019;99(3):1527–1573.
23. Provis JM, Dubis AM, Maddess T, Carroll J. Adaptation of the central retina for high acuity vision: cones, the fovea and the avascular zone. *Prog Retin Eye Res*. 2013;35:63–81.
24. Reiter GS, Schwarzenbacher L, Schartmüller D, et al. Influence of lens opacities and cataract severity on quantitative fundus autofluorescence as a secondary outcome of a randomized clinical trial. *Sci Rep*. 2021;11(1):12685.
25. Reiter GS, Told R, Schlanitz FG, et al. Impact of Drusen Volume on Quantitative Fundus Autofluorescence in Early and Intermediate Age-Related Macular Degeneration. *Invest Ophthalmol Vis Sci*. 2019;60(6):1937–1942.
26. Chen L, Messinger JD, Ferrara D, Freund KB, Curcio CA. Fundus Autofluorescence in Neovascular Age-Related Macular Degeneration: A Clinicopathologic Correlation Relevant to Macular Atrophy. *Ophthalmol Retin*. 2021;2(11):1085–1096.
27. von Rückmann A, Fitzke FW, Fan J, Halfyard A, Bird AC. Abnormalities of fundus autofluorescence in central serous retinopathy. *Am J Ophthalmol*. 2002;133(6):780–786.
28. Freund KB, Mrejen S, Jung J, Yannuzzi LA, Boon CJF. Increased fundus autofluorescence related to outer retinal disruption. *JAMA Ophthalmol*. 2013;131(12):1645–1649.
29. Ablonczy Z, Higbee D, Grey AC, Koutalos Y, Schey KL, Crouch RK. Similar molecules spatially correlate with lipofuscin and N-retinylidene-N-retinylethanolamine in the mouse but not in the human retinal pigment epithelium. *Arch Biochem Biophys*. 2013;539(2):196–202.
30. Anderson DMG, Messinger JD, Patterson NH, et al. Lipid Landscape of the Human Retina and Supporting Tissues Revealed by High-Resolution Imaging Mass Spectrometry. *J Am Soc Mass Spectrom*. 2020;31(12):2426–2436.
31. Wing GL, Blanchard GC, Weiter JJ. The topography and age relationship of lipofuscin concentration in the retinal pigment epithelium. *Invest Ophthalmol Vis Sci*. 1978;17(7):601–607.
32. Owsley C, Jackson GR, White M, Feist R, Edwards D. Delays in rod-mediated dark adaptation in early age-related maculopathy. *Ophthalmology*. 2001;108(7):1196–1202.
33. Curcio CA, Owsley C, Jackson GR. Spare the rods, save the cones in aging and age-related maculopathy. *Invest Ophthalmol Vis Sci*. 2000;41(8):2015–2018.
34. von der Emde L, Pfau M, Thiele S, et al. Mesopic and Dark-Adapted Two-Color Fundus-Controlled Perimetry in Choroidal Neovascularization Secondary to Age-Related Macular Degeneration. *Transl Vis Sci Technol*. 2019;8(1):7.
35. Kim IT, Choi JB. Melanosomes of retinal pigment epithelium–distribution, shape, and acid phosphatase activity. *Korean J Ophthalmol*. 1998;12(2):85–91.
36. Taubitz T, Fang Y, Biesemeier A, Julien-Schraermeyer S, Schraermeyer U. Age, lipofuscin and melanin oxidation affect fundus near-infrared autofluorescence. *EBioMedicine*. 2019;48:592–604.
37. Grieve K, Gofas-Salas E, Ferguson RD, Sahel JA, Paques M, Rossi EA. In vivo near-infrared autofluorescence imaging of retinal pigment epithelial cells with 757 nm excitation. *Biomed Opt Express*. 2018;9(12):5946–5961.
38. Keilhauer CN, Delori FC. Near-infrared autofluorescence imaging of the fundus: visualization of ocular melanin. *Invest Ophthalmol Vis Sci*. 2006;47(8):3556–3564.
39. Sarks SH, Arnold JJ, Killingsworth MC, Sarks JP. Early drusen formation in the normal and aging eye and their relation to age related maculopathy: a clinicopathological study. *Br J Ophthalmol*. 1999;83(3):358–368.
40. Sarks S, Cherepanoff S, Killingsworth M, Sarks J. Relationship of Basal laminar deposit and membranous debris to the clinical presentation of early age-related macular degeneration. *Invest Ophthalmol Vis Sci*. 2007;48(3):968–977.
41. Sura AA, Chen L, Messinger JD, et al. Measuring the Contributions of Basal Laminar Deposit and Bruch's Membrane in Age-Related Macular Degeneration. *Invest Ophthalmol Vis Sci*. 2020;61(13):19.

Investigative Ophthalmology & Visual Science

42. Chen L, Messinger JD, Kar D, Duncan JL, Curcio CA. Biometrics, Impact, and Significance of Basal Linear Deposit and Subretinal Drusenoid Deposit in Age-Related Macular Degeneration. *Invest Ophthalmol Vis Sci*. 2021;62(1):33.
43. Julien S, Schraermeyer U. Lipofuscin can be eliminated from the retinal pigment epithelium of monkeys. *Neurobiol Aging*. 2012;33(10):2390–2397.
44. Julien-Schraermeyer S, Illing B, Tschulakow A, et al. Penetration, distribution, and elimination of remofuscin/soraprazan in Stargardt mouse eyes following a single intravitreal injection using pharmacokinetics and transmission electron microscopic autoradiography: Implication for the local treatment of Stargardt's disease and dry age-related macular degeneration. *Pharmacol Res Perspect*. 2020;8(6):e00683.
45. Ma L, Kaufman Y, Zhang J, Washington I. C20-D3-vitamin A slows lipofuscin accumulation and electrophysiological retinal degeneration in a mouse model of Stargardt disease. *J Biol Chem*. 2011;286(10):7966–7974.
46. Racz B, Varadi A, Kong J, et al. A non-retinoid antagonist of retinol-binding protein 4 rescues phenotype in a model of Stargardt disease without inhibiting the visual cycle. *J Biol Chem*. 2018;293(29):11574–11588.
47. Chen M, Rajapakse D, Fraczek M, Luo C, Forrester J V, Xu H. Retinal pigment epithelial cell multinucleation in the aging eye - a mechanism to repair damage and maintain homoeostasis. *Aging Cell*. 2016;15(3):436–445.
48. Starnes AC, Huisingh C, McGwin GJ, et al. Multi-nucleate retinal pigment epithelium cells of the human macula exhibit a characteristic and highly specific distribution. *Vis Neurosci*. 2016;33:e001.
49. Lacroix B, Maddox AS. Cytokinesis, ploidy and aneuploidy. *J Pathol*. 2012;226(2):338–351.
50. Ts'o MO, Friedman E. The retinal pigment epithelium. 3. Growth and development. *Arch Ophthalmol (Chicago, Ill 1960)*. 1968;80(2):214–216.
51. Delori FC, Fleckner MR, Goger DG, Weiter JJ, Dorey CK. Autofluorescence distribution associated with drusen in age-related macular degeneration. *Invest Ophthalmol Vis Sci*. 2000;41(2):496–504.
52. Neubauer AS, Thiel M, Priglinger S, et al. Mapping of the retinal pigment epithelium in exudative age related macular degeneration. *Graefe's Arch Clin Exp Ophthalmol = Albr von Graefes Arch fur Klin und Exp Ophthalmol*. 2006;244(3):342–351.
53. Miura M, Makita S, Sugiyama S, et al. Evaluation of intraretinal migration of retinal pigment epithelial cells in age-related macular degeneration using polarimetric imaging. *Sci Rep*. 2017;7(1):3150.
54. Balaratnasingam C, Messinger JD, Sloan KR, Yannuzzi LA, Freund KB, Curcio CA. Histologic and Optical Coherence Tomographic Correlates in Drusenoid Pigment Epithelium Detachment in Age-Related Macular Degeneration. *Ophthalmology*. 2017;124(5):644–656.
55. Zanzottera EC, Messinger JD, Ach T, Smith RT, Freund KB, Curcio CA. The Project MACULA Retinal Pigment Epithelium Grading System for Histology and Optical Coherence Tomography in Age-Related Macular Degeneration. *Invest Ophthalmol Vis Sci*. 2015;56(5):3253–3268.
56. Cao D, Leong B, Messinger JD, et al. Hyperreflective Foci, Optical Coherence Tomography Progression Indicators in Age-Related Macular Degeneration, Include Transdifferentiated Retinal Pigment Epithelium. *Invest Ophthalmol Vis Sci*. 2021;62(10):34.

Investigative Ophthalmology & Visual Science